The Astrophysical Journal, 603:127–134, 2004 March 1

DISCOVERY OF ANOTHER PECULIAR RADIAL DISTRIBUTION OF BLUE STRAGGLERS IN GLOBULAR CLUSTERS: THE CASE OF 47 TUCANAE[1]

Francesco R. Ferraro,[2] Giacomo Beccari,[2] Robert T. Rood,[3] Michele Bellazzini,[4] Alison Sills,[5] and Elena Sabbi[2]
Received 2003 July 24; accepted 2003 November 10

ABSTRACT

We have used the high-resolution Wide Field Planetary Camera (WFPC2) on the *Hubble Space Telescope* (*HST*) and wide-field ground-based observations to construct a catalog of blue straggler stars (BSSs) in the globular cluster 47 Tuc spanning the entire radial extent of the cluster. The BSS distribution is highly peaked in the cluster center, rapidly decreases at intermediate radii, and finally rises again at larger radii. The observed distribution closely resembles that discovered in M3 by Ferraro and coworkers. To date, complete BSS surveys covering the full radial extent (from *HST* for the center and wide-field CCD, ground-based observations for the exterior) have only been performed for these two clusters. Both show a bimodal radial distribution despite their different dynamical properties. BSS surveys covering the full spatial extent of more globular clusters are clearly required to determine how common bimodality is and what its consequences are for theories of BSS formation and cluster dynamics.

Subject headings: binaries: close — blue stragglers — globular clusters: individual (47 Tucanae) — stars: evolution

1. INTRODUCTION

Blue straggler stars (BSSs) are found primarily in star clusters, where they appear as a sparsely populated extension of the main sequence (MS) above the turnoff point. Superficially they appear to be MS stars with masses larger than expected for the cluster at its turnoff age. There are two proposed mechanisms thought to produce BSSs: the first is mass exchange in a binary system, and the second is the merger of two stars induced by stellar interactions (either single or in binaries) in a dense stellar environment. Globular cluster cores are obvious targets for BSSs, not only because of their high stellar density, but because primordial binaries in the clusters may well have sunk to the cores.

With the advent of the *Hubble Space Telescope* (*HST*) it became possible for the first time to search dense cluster cores for BSSs. Searches in the ultraviolet (UV) can be particularly effective, not because BSSs are especially bright in the UV, but because the red giants are faint in the UV. The photometric blends which mimic BSSs in visible color-magnitude diagrams (CMDs) are far less problematic in the best UV CMD planes, so it is possible to obtain complete BSS samples in even the densest cores. With *HST*, the densest cluster cores are the obvious places to search for BSSs, and there have been few systematic searches for BSSs in the outer parts of clusters in recent years. Indeed, only one cluster, M3, has been adequately surveyed for BSSs over its entire radial extent (Ferraro et al. 1993, 1997).

Since it is a massive cluster with high central density, 47 Tuc is an obvious target for a BSS search, and its core has been the subject of several earlier investigations (Guhathakurta et al. 1992; de Marchi, Paresce, & Ferraro 1993; Ferraro et al. 2001; Knigge et al. 2002). These studies have covered only a fraction of the core, because they used either the Faint Object Camera or just the planetary camera (PC) of WFPC2. Albrow et al. (2001) found BSSs in their WFPC2 search for eclipsing binaries in the core of 47 Tuc. BSSs have also been studied outside the core of 47 Tuc by Sills et al. (2000), who also modeled the BSS formation rate. Kaluzny et al. (1998) note several BSS candidates in their CMD of 47 Tuc, and there are clear BSS candidates in the Strömgren photometry of Grundahl, Stetson, & Andersen (2002). Only a small part of the cluster exterior was covered by these studies.

With new wide-field imagers on ground-based telescopes at sites with excellent seeing, it is now possible to perform BSS surveys that yield complete samples over the entire extent of the cluster. Here we present results covering both the full cluster core using WFPC2 and the cluster exterior using the wide field imager (WFI) at the ESO 2.2 m telescope.

2. OBSERVATIONS AND DATA ANALYSIS

2.1. *The Data Set*

The photometric data used here consist of two sets:

1. *High-resolution set.*—A series of public *HST* WFPC2 images were taken through the UV filters F218W and F439W(*B*). The images have been retrieved from the ESO Space Telescope-European Coordinating Facility (ST-ECF) Science Archive, an automatic archive association procedure that allows retrieval of a set of images taken with the same filter and under similar conditions. The images are automatically combined and cleaned of cosmic rays. The first part of this data set (specifically the PC) has been already published in Ferraro et al. (2001). Here we present the analysis of the entire data set (including the PC, WF2, WF3, and WF4). Information about the observing epochs, proposal ID number, filter, and number of exposures can be found in Table 1 of Ferraro et al. (2001). The

[1] Based on observations with the NASA/ESA *HST*, obtained at the Space Telescope Science Institute, which is operated by AURA, Inc., under NASA contract NAS5-26555. Also based on WFI observations collected at the ESO, La Silla, Chile, within the observing programs 62.L-0354 and 64.L-0439.

[2] Dipartimento di Astronomia Università di Bologna, Via Ranzani, 1, Bologna I-40127, Italy; ferraro@bo.astro.it.

[3] Astronomy Department, University of Virginia, Charlottesville, VA 22903-0818; rtr@virginia.edu.

[4] INAF, Osservatorio Astronomico di Bologna, Via Ranzani, 1, Bologna I-40127, Italy; bellazzini@bo.astro.it.

[5] Department of Physics and Astronomy, McMaster University, 1280 Main Street West, Hamilton, ON L8S 4M1, Canada; asills@mcmaster.ca.

photometric reductions of the high-resolution images were carried out using ROMAFOT (Buonanno et al. 1983), a package developed to perform accurate photometry in crowded fields and specifically optimized to handle undersampled point spread functions (PSFs) (Buonanno & Iannicola 1989), as in the case of the *HST* WF chips.

PSF-fitting instrumental magnitudes have been obtained using the standard procedure described in Ferraro et al. (1997, 2001). The final catalog of the F218W and F439W magnitudes was calibrated by using the zero points listed by Holtzman et al. (1995).

2. *Wide field set.*—A complementary set of multifilter (B, V, and I) wide-field images was secured during an observing run at the 2.2 m ESO-MPI telescope at ESO (La Silla) in 1999 July, using the WFI. An additional dataset of public WFI images were also retrieved from the ESO/ST-ECF Science Archive. The WFI has exceptional imaging capabilities; each image consists of a mosaic of eight CCD chips (each with a field of view of $8' \times 16'$), giving a global field of view (FOV) of $33' \times 34'$.

The raw WFI images were corrected for bias and flat field, and the overscan region was trimmed using standard IRAF[6] tools. The PSF-fitting procedure was performed independently on each V, B, and I image, using DoPHOT (Schechter, Mateo, & Saha 1993). For each passband at least seven exposures were combined and the resulting magnitudes transformed to the same (instrumental) photometric system; stars in common were then averaged, with the requirement that only stars successfully measured in at least three images per filter were included. A final catalog listing the instrumental B, V, I magnitudes for all the stars in each CCD field was thus obtained.

2.2. *Astrometry*

The *HST*+WFI catalog was placed on the absolute astrometric system by adopting the procedure already described in previous papers (see Ferraro et al. 2001, 2003a). The new astrometric Guide Star Catalog (GSCII)[7] was used to search for astrometric standard stars lying in the WFI image FOV. Several hundred GSCII reference stars have been found in the WFI FOV, allowing an accurate absolute positioning of the image. In order to derive an astrometric solution for each of the eight WFI chips, we used a program specifically developed at the Bologna Observatory (P. Montegriffo et al. 2004, in preparation). Then, a few hundred stars in the overlapping area between the WFI and the WFPC2 FOVs were used as secondary astrometric standards in order to place the *HST* catalog in the absolute astrometric system. At the end of the entire procedure, the rms residuals were of the order of $\sim 0\farcs3$ in both right ascension and declination, and we take this value as representative of the astrometric accuracy.

We used our standard technique (Montegriffo et al. 1995; Ferraro et al. 1999, 2001, 2003a) to find the center of gravity ($C_{\rm grav}$). The barycenter of resolved stars is compatible (within $1''$–$2''$) with the center of luminosity, $C_{\rm lum}$, listed by Djorgovski & Meylan (1993). Thus, in the following we use their value as the center: $\alpha_{\rm J2000.0} = 00^{\rm h}24^{\rm m}05\fs20$, $\delta_{\rm J2000.0} = -72^\circ 04' 51''$.

[6] IRAF is distributed by the National Optical Astronomy Observatory, which is operated by the Association of Universities for Research in Astronomy, Inc., under cooperative agreement with the National Science Foundation.

[7] Available at http://www-gsss.stsci.edu/gsc/gsc2/GSC2home.htm.

3. DEFINITION OF THE SAMPLES

In order to avoid spurious effects due to incompleteness of the ground-based observations in the crowded central region of the cluster, we restricted the WFI sample to the outer region, $r > 130''$ (hereafter simply the WFI sample). In the inner region, $r < 130''$, our sample included only stars in the WFPC2 FOV (hereafter the *HST* sample). This sample takes advantage of the superior capability of UV observations in detecting BSSs (Ferraro et al. 1999, 2001) in the overcrowded central regions of high density clusters. The CMDs derived from these samples are shown in Figures 1 and 2.

3.1. *The BSS Selection*

Since the two data sets have been observed in different photometric bands, different selection boxes have to be defined to isolate the populations in the two CMDs. The definition of the BSS sample is quite natural in the UV CMD (Fig. 1), since, as is usually seen, in these planes the BSSs define a quite distinct sequence spanning $\sim$3 mag. Approximately 100 BSSs have been identified in the *HST* WFPC2 FOV. However, as in our previous studies of M3 and M80 (respectively: Ferraro et al. 1997, hereafter F97; Ferraro et al. 1999), to avoid any possible contamination due to blends, incompleteness etc., here we limit our analysis to the brightest portion of the BSS sequence. The faint threshold of the BSS selection box was chosen to be $m_{218} < 18.7$. This limit is nearly 1 mag brighter than the cluster MS turnoff (TO) in the UV plane, to avoid any spurious effect due to blends. The adopted selection box for the BSSs in the *HST* sample is shown in Figure 1. A total of 59 bright-BSSs (b-BSSs) have been counted in this selection box.

In order to make a meaningful BSS selection in the WFI sample, we converted the magnitude extension of the box defined in the UV plane into the ground-based (B, $B-V$) and (B, $B-I$) planes. The corresponding values have been computed by using the B filter, which is common to both datasets (since the F439W WFPC2 filter is approximately a B filter). To do this we first aligned the two CMDs in the ($m_{\rm F439W}$, $m_{\rm F218W}-m_{\rm F439W}$) and ($B$, $B-V$) planes by using the subgiant-branch (SGB) and the horizontal-branch (HB) levels as a reference, and then we determined the distribution of the selected bright BSSs in B magnitude. This procedure gives a value of $B \sim 17.3$ and $\sim$15 for the faint and the bright threshold, respectively, of the BSS box in the WFI sample.

The color limits of the BSS box in the ground-based planes have been chosen to minimize the possibility of field contamination. The red edge has been assumed to be at $B-V = 0.5$, where a significative decrease of the galaxy field contribution is expected (see, e.g., Fig. 2 in Unavane, Wyse, & Gilmore 1996; Fig. 4 in Lemon et al. 2004). The blue edge has been chosen in order to exclude a few blue objects that lie significantly outside the BSS sequence (see Fig. 2*a*). This selection includes the bulk of the BSS population, although a few evolved BSSs might be lost in the region dominated by the field population. However, as discussed in previous papers, the number of lost BSSs is certainly small (see, for example, the case of M3; Ferraro et al. 1993, 1997). We emphasize that even slightly different assumptions in the definition of the selection boxes would not alter the main results presented in this paper. With these limits, an appropriate selection box for the bright BSSs has been defined in both the optical planes (see Fig. 2). A preliminary selection of possible BSSs was done in the (B, $B-V$) plane, but the final

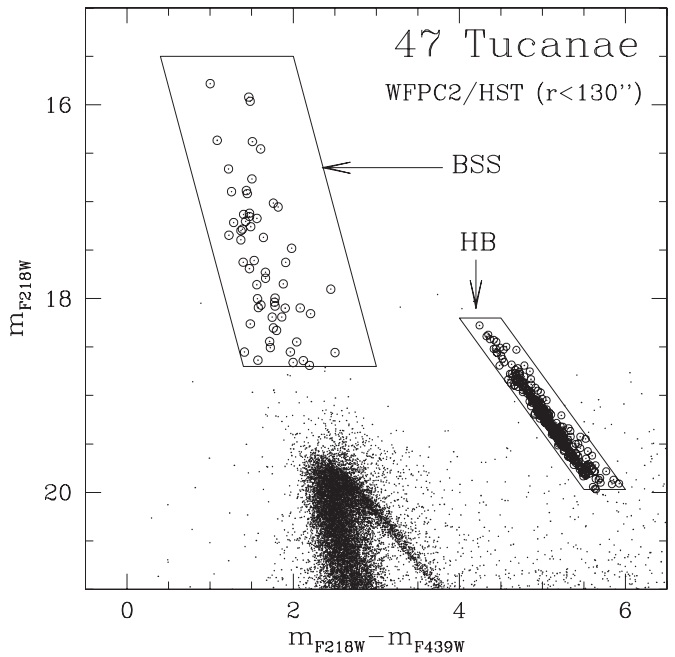

FIG. 1.—Plot of (m_{218}, $m_{218}-m_{439}$) CMD for the central region of 47 Tuc ($r < 130''$) from WFPC2 observations. The two selection boxes for the BSS and the reference (HB) populations are shown, and the selected stars marked with circles.

selection was done using both the (B, $B-V$) and (B, $B-I$) CMDs. Thus, only the 57 objects that lie in the BSS selection boxes in both CMDs have been selected.

Figure 3 compares the BSSs selected in the *HST* and WFI samples, which are considered below. In order to make the two samples completely homogeneous, the faintest six BSSs in the *HST* sample that fall just below the adopted threshold ($B \sim 17.3$) have been excluded. The final sample consists of 53 BSSs in the *HST* sample and 57 BSSs in the WFI sample (for a total of 110 objects).

3.2. *The Reference Population*

In order to study the behavior of the BSSs with respect to the normal stars in the cluster, we must select a reference population that is assumed to trace the cluster stars. As discussed in previous papers (see, e.g., Ferraro et al. 2003b), the most *natural* reference population in the UV CMDs is the HB, since it is well separated from the other branches, and HB stars are quite bright in most CMD planes (see Fig. 1).

The selection of the HB stars is quite easy in both planes, since they are a well-defined visible clump of stars in both the UV (see Fig. 1; and Fig. 2 in Ferraro et al. 2001) and the ground-based CMDs (see Fig. 2). Again the HB star selection is defined independently in all the CMDs and is designed to include the bulk of the HB population. The HB box shown in Figure 1 and the selection shown in Figure 2 assure the inclusion of the bulk of the HB stars; small differences in the assumptions on the shape of the box would only include or exclude a few stars. For example, a fainter threshold for the

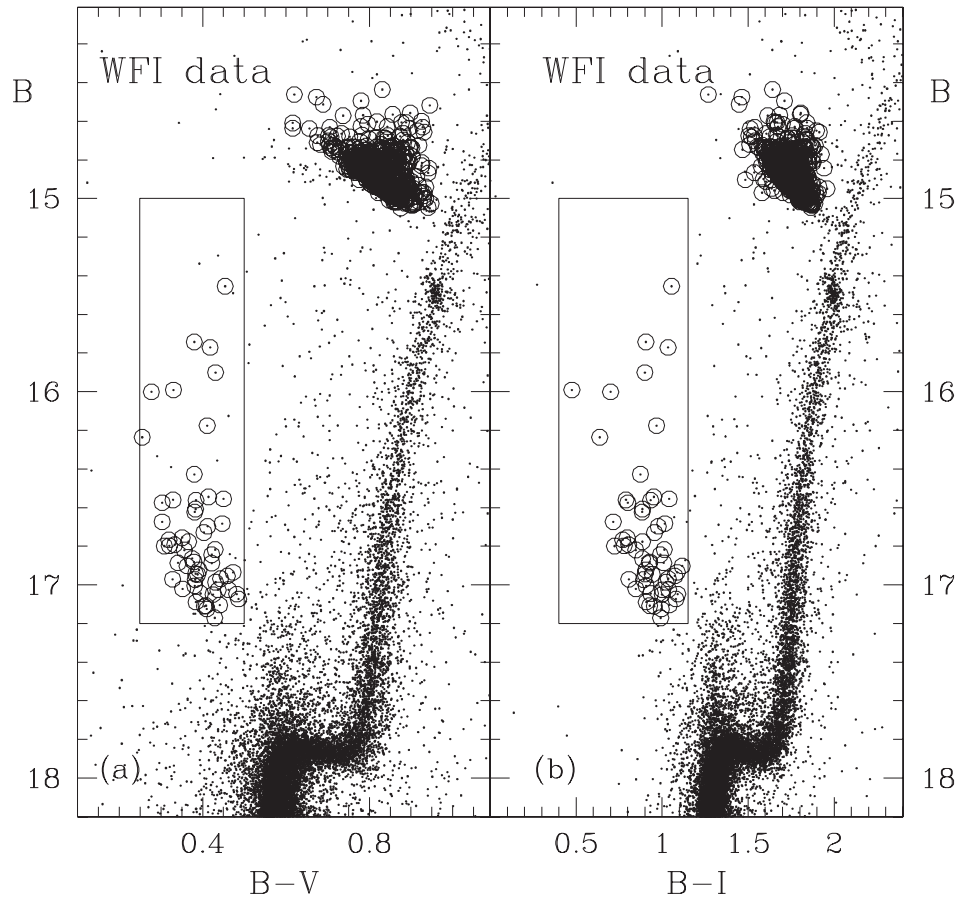

FIG. 2.—Plots of (*a*) B, $B-V$ and (*b*) B, $B-I$ CMDs for the external part of 47 Tuc ($130'' < r < 1500''$) from ground-based WFI observations. As in Fig. 1, stars selected in the BSS (*inside box*) and the reference (HB) populations are marked with circles.

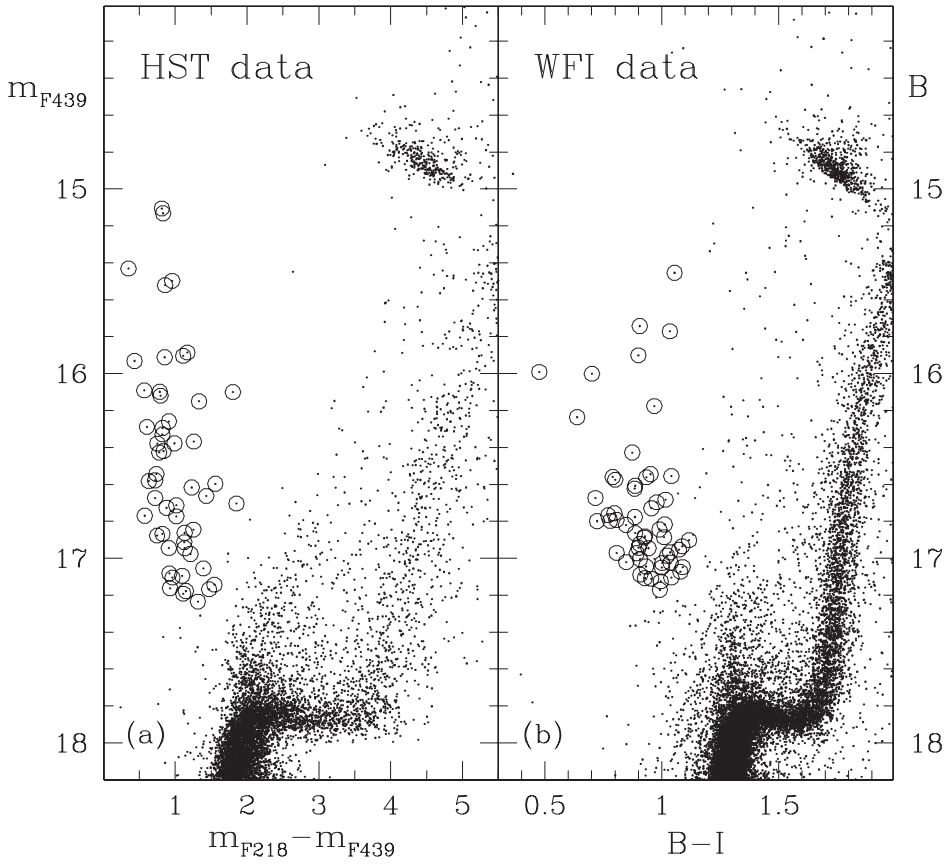

FIG. 3.—Direct comparison between (*a*) the *HST* and (*b*) the ground-based WFI sample ; stars selected in the BSS population are marked with circles. As can be seen, the selected BSS samples are fully homogeneous.

HB box in the UV plane would include a few scattered stars that might be red giant branch (RGB) stars. In the ground-based planes (Fig. 2), we designed an appropriate box to avoid the inclusion a small sequence of underluminous HB stars that clearly lie below the zero-age HB in Figure 2*a*. Again, the inclusion of these stars (which are less than a few percent of the global HB population) does not affect our conclusions in any way.

Following the criteria described above, a total sample of 314 and 581 HB stars have been counted in the HB selection boxes in the *HST* and WFI samples, respectively. The global sample of 116 b-BSSs and 895 HB stars spans almost the entire radial extension of the cluster ($0'$ to $23'$ from the cluster center) and is the largest sample ever published for 47 Tuc.

3.3. *Field Contamination*

Galaxy foreground contamination in the BSS region is negligible thanks to the selection in color ($B-V < 0.5$; see Fig. 4 in Lemon et al. 2004, Fig. 2 in Unavane et al. 1996). By using the star counts of Ratnatunga & Bahcall (1985), we estimate that $\sim$100 field stars with $B-V < 0.8$ and $13 < V < 17$ are expected in the WFI FOV. Figure 2 in Unavane et al. (1996) and Figure 4 in Lemon et al. (2004) show that the bulk of the Galaxy foreground stars are expected to have $B-V > 0.5$.

The brighter portion of the RGB of the Small Magellanic Cloud (SMC) field population is clearly visible in our CMD at $B = 18.2$, $B-V = 1.6$. Moreover, the main contribution of the SMC background stars is expected at magnitudes significantly fainter than the BSS selection box (see Fig. 1 in Zoccali et al. 2001). In any case, the BSS selection box is located in the region between the MS of young stars and the evolved RGB stars (compare the BSS selection box with Fig. 10 in Momany et al. 2001), where only a few SMC field stars are expected. In accord with the above considerations, no correction has been applied to the BSS counts.

4. RESULTS

As a first step, the radial distribution of the 110 b-BSSs has been compared to that of the reference population. The cumulative radial distribution for the 110 b-BSSs and the 895 HB stars are plotted in Figure 4*a* as a function of the projected distance from the cluster center. As can be seen, the behavior of the two distributions is not monotonic since the BSSs appear to be more concentrated than the HB stars in the central region and less concentrated than the HB stars in the outer region. Note that the shoulder visible in the radial distribution shown in Figure 4*a* is due to the *HST*–ground-based sample transition. As discussed above, we conservatively decided to consider in the region $r < 130''$ only stars observed with *HST*. Because of the shape of the WFPC2 FOV, there is a region at $r \sim 110''-130''$ where only a few stars can be detected. This region is indicated by the vertical shaded region in Figure 4*a*. The assumption of using only the *HST* sample in the innermost region of the cluster is, in our opinion, the safest possible choice since the ground-based magnitudes could still be severely affected by the crowded conditions at this distance from the cluster center. Note that this shoulder effect vanishes when the BSS population is scaled to a reference population (HB or RGB) or fractional luminosity as we do below.

The effect is better illustrated in Figure 4*b*, in which the radial distributions for two *HST* and WFI subsamples are

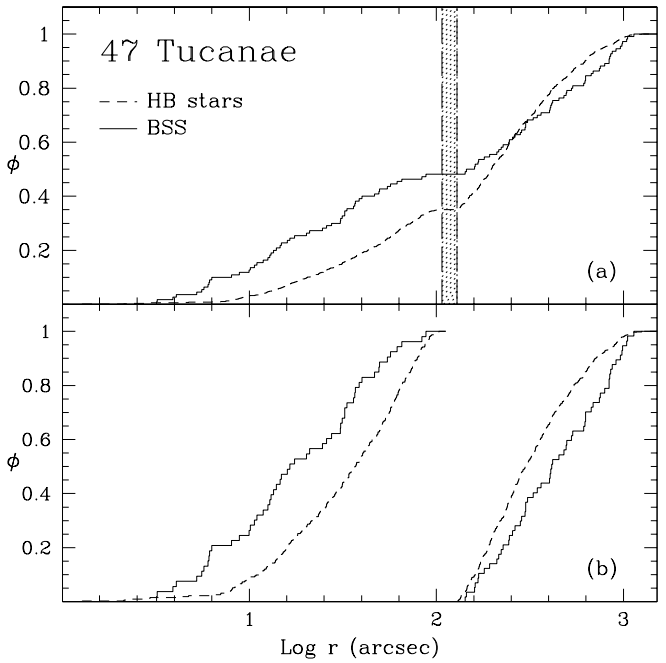

FIG. 4.—(*a*) Cumulative radial distributions for the b-BSSs (*solid line*) and the HB stars (*dashed line*) as a function of their projected distance, *r*, from the cluster center for the global sample. The vertical shaded region separates the cluster regions observed with *HST* from the regions observed from the ground. (*b*) Same as (*a*), but for two radial subsamples.

shown separately. As can be seen, the BSSs are clearly more concentrated in the central region (*HST* sample) and less concentrated in the outer region (WFI sample) with respect to the reference HB population. A Kolmogorov-Smirnov test has been applied to the distributions to check the statistical significance of the differences. The test yields a probability of 99.96% (more than 3 σ level of confidence) and 98.86% ($\sim$2.5 σ level of confidence) that the b-BSS population has a different radial distribution with respect to the HB stars. This distribution closely resembles that already observed in M3 (Ferraro et al. 1993, hereafter F93; F97): indeed, Figure 4*b* is almost exactly the same as Figure 7 in F97. We accordingly follow the procedure described in F93 (also applied in F97), in which the surveyed area is divided into a set of concentric annuli. Thus, 11 concentric annuli (each containing $\sim$10% of the reference population) have been defined (see Table 1). The number of BSSs and HB stars are then counted in each annulus. The first observable quantity that can be measured in each annulus is the relative frequency $N_{\rm BSS}/N_{\rm HB}$.

Figure 5*a* shows the distribution of this ratio as a function of the effective radius of each annulus. The distribution is clearly bimodal with the highest value in the innermost annulus. From this quite large value ($N_{\rm BSS}/N_{\rm HB} \sim 0.4$) the relative frequency significantly decreases to less than 0.1 as *r* increases and then slowly increases in the outer region up to $\sim$0.3. Again this trend closely resembles that discovered in M3 by F97. In order to better analyze this trend we have computed the specific frequency, *R*, i.e., the relative frequency of BSSs and HB stars, normalized to the fraction of luminosity sampled in each annulus. The fraction of light sampled in each annulus has been computed from the cluster brightness profile, and appropriately scaled to the fraction of area covered by the observations in each annulus.

The original definitions by F93 are

$$R_{\rm BSS} = \frac{(N_{\rm BSS}/N_{\rm BSS}^{\rm tot})}{(L^{\rm sample}/L_{\rm tot}^{\rm sample})},$$

$$R_{\rm HB} = \frac{(N_{\rm HB}/N_{\rm HB}^{\rm tot})}{(L^{\rm sample}/L_{\rm tot}^{\rm sample})}.$$

The numbers of BSSs and HB stars in each annulus, the $N_{\rm BSS}/N_{\rm HB}$ ratio, the sampled luminosity and the specific frequencies, as defined above, are listed in Table 1. The specific frequency of BSSs as a function of the distance from the cluster center is then plotted in Figure 5*b* and compared with the corresponding one for the HB "reference" stars. As can be seen, the HB specific frequency remains essentially constant over the surveyed area since the fraction of HB stars (as any post-MS stage) in each annulus strictly depends on the fraction of luminosity sampled in that annulus (see the relation in Renzini & Buzzoni 1986; eq. [2] in Ferraro et al. 2003b). In contrast, the BSS specific frequency reaches its maximum at the center of the cluster then decreases to an approximately constant value in the range 100″–500″ from the cluster center and then rises again. This behavior fully confirms the trend shown in Figure 5*a* and suggests that dynamical events and/or a formation mechanism shape the radial distribution of the BSSs in the cluster (Mapelli et al. 2004).

To further demonstrate the similarity with M3 and to study possible differences we show BSS specific frequencies for the two clusters in Figure 6. The radial coordinate has been expressed as a function of the core radius r_c. Using our

TABLE 1
NUMBERS AND SPECIFIC FREQUENCIES FOR BSS AND HB STARS

r (arcsec)	$N_{\rm BSS}$	$N_{\rm HB}$	$N_{\rm BSS}/N_{\rm HB}$	$L_{\rm annulus}/L_{\rm tot}$	$R_{\rm BSS}$	$\epsilon_{\rm BSS}$	$R_{\rm HB}$	$\epsilon_{\rm HB}$
0–17	27	71	0.38	0.09	2.64	0.57	0.85	0.11
17–40	16	99	0.16	0.12	1.16	0.31	0.88	0.09
40–130	10	144	0.07	0.14	0.67	0.22	1.18	0.11
130–170	6	78	0.09	0.10	0.53	0.22	0.84	0.10
170–230	6	110	0.07	0.11	0.48	0.20	1.09	0.11
230–290	6	94	0.07	0.08	0.65	0.27	1.26	0.14
290–370	7	77	0.09	0.08	0.77	0.30	1.04	0.12
370–490	7	77	0.08	0.09	0.72	0.28	0.98	0.12
490–680	9	79	0.13	0.09	0.92	0.32	0.99	0.12
680–900	9	38	0.23	0.06	1.31	0.45	0.68	0.11
900–1462	7	28	0.29	0.03	2.52	0.98	1.24	0.24

NOTE.—$\epsilon_{\rm BSS}$ and $\epsilon_{\rm HB}$ are the errors for $R_{\rm BSS}$ and $R_{\rm HB}$, respectively.

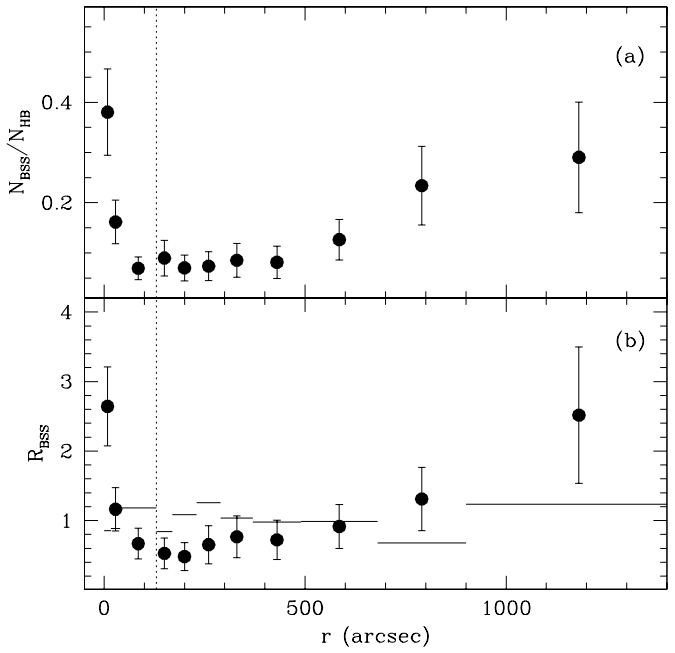

FIG. 5.—(*a*) Relative frequency of BSSs with respect to HB stars plotted as a function of the distance from the cluster center for each of the 11 concentric annuli defined in the text. (*b*) Specific frequency of BSSs (see text). The horizontal lines show the specific frequency for the HB reference population. The vertical dotted lines distinguish the cluster regions observed with *HST* from the regions observed from the ground.

observed star counts we have found values of $r_c = 21''$ and $24''$ for 47 Tuc and M3, respectively. In order to derive the core radius we followed the same procedure shown in Ferraro et al. (2003a). All stars brighter than the cluster main sequence turnoff have been used to derive the star density profile, which was then fitted by the projected star density obtained from a standard isotropic single-mass King model. The full discussion of the star density profile for both (and a few other) clusters will be presented in a forthcoming paper (F. Ferraro et al. 2004, in preparation). A typical uncertainty of $\pm 2''$ can be assumed in the r_c determination. Note that the value assumed for 47 Tuc is consistent with that ($r_c = 24'' \pm 2''$) recently obtained by Howell, Guhathakurta, & Gilliland (2000), in a review discussing the most recent determinations of the core radius of 47 Tuc using *HST*. Some points about Figure 6 are worth noting. (1) The central values are similar. (2) While the BSS specific frequency decreases in both clusters as r increases from 0 to $\sim 4r_c$, the decrease is much larger in M3. In 47 Tuc it decreases by a factor of 5.5, dropping from 2.64 to 0.48; in M3 the drop is by a factor of 15 (from 2.76 to 0.2). (3) The main difference in the two distributions is that the specific frequency minimum in 47 Tuc appears to be much broader than that observed in M3. In 47 Tuc, the depletion zone extends from $\sim 4r_c$ to $(20–22)r_c$, with the upturn of the BSS density occurring at $\sim 25r_c$, while in M3 the BSS specific frequency is already rising at $\sim 8r_c$.

5. DISCUSSION

F97 argued that the bimodal distribution of BSSs in M3 is evidence that two formation scenarios were at action in the same cluster: the exterior BSSs (EBSSs) arising from mass transfer in primordial binaries, and the central BSSs (CBSSs) from stellar interactions which lead to mergers. As had been earlier noted by Bailyn & Pinsonneault (1995), the EBSS and CBSS luminosity functions differed in the sense theoretically expected for the two mechanisms.

One difficulty with primordial binaries as a source for the EBSSs is that one would ordinarily expect that they would have settled to the cluster centers, since relaxation times are typically less than 1 Gyr (Djorgovski 1993). Simulations to address the question of how many primordial binaries can form in the external regions of the cluster and how long primordial binaries with mass approaching twice the turnoff mass could remain in the outer parts of a cluster are now in progress (Mapelli et al. 2004).

Sigurdsson, Davies, & Bolte (1994) offered another explanation for the bimodal BSS distribution in M3. They suggested that the EBSSs were formed in the core and then ejected into the outer regions by the recoil from the interactions. Those binaries that get kicked out to a few r_c rapidly drift back to the center of the cluster because of mass segregation, leading to a concentration of BSSs near the center and a paucity of BSSs in the outer parts of this region. More energetic kicks will take the BSSs to larger distances; these stars require much more time to drift back toward the core and may account for the overabundance of BSSs at larger distances.

How does the discovery of a bimodal radial distribution of BSSs in 47 Tuc affect these arguments? Dynamically 47 Tuc is quite different from M3: its central density is 40 times larger (Pryor & Meylan 1993), and its core is rich in X-ray binaries, millisecond pulsars, and other interaction products (Ferraro et al. 2001; Grindlay et al. 2001; Camilo et al. 2000; Edmonds et al. 2003). We have already shown that CBSS populations cannot be characterized by a simple parameter like collision rate (Ferraro et al. 2003b), so the fact that CBSSs in 47 Tuc and M3 have comparable specific frequencies should not come as a surprise.

It should be noted that a BSS specific frequency upturn similar to that observed in 47 Tuc and M3 has also been detected in M55 (Zaggia, Piotto, & Capaccioli 1997). This is of particular significance because M55 has a low central density, 0.1 that of M3. Note that although the data set presented by Zaggia et al. (1997) for M55 are ground-based observations and only covered a quadrant of the cluster, there is at least preliminary evidence that an upturn is also present in a low-density cluster like M55. We note that the effect found by Zaggia et al. (1997) in M55 could be even stronger, since ground-based observations tend to hide BSSs in the central

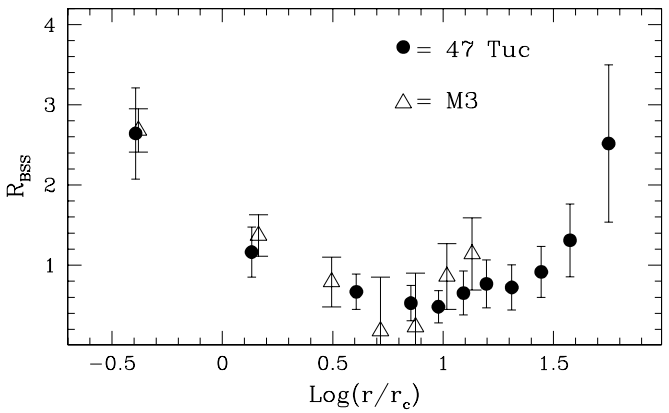

FIG. 6.—Specific frequency of BSSs in 47 Tuc (*filled circles*) compared with that found in M3 (*open triangles*). The radial coordinate is expressed in units of core radii r_c.

region of the cluster. For example, ground-based observations of the center of M3 led Bolte, Hesser, & Stetson (1993) to claim depletion of BSSs in the center, although *HST* observations eventually found a peak. M55 is surely less concentrated than M3, but still-intermediate crowding conditions and the presence of highly saturated giants in the center can produce some level of incompleteness at the BSS level.

The implications of the bimodality and relatively large populations of EBSSs are not yet clear, beyond the fact that EBSSs may be fairly common and form in diverse clusters. If the BSS bimodality in M55 is confirmed, we will be faced with the result that clusters with central densities ranging over a factor of 400 can produce a bimodal BSS distribution. Any dynamical model like that of Sigurdsson et al. (1994) would seem more applicable to 47 Tuc than M3. It would be a real stretch to reach the dynamical conditions in M55.

Given these factors it seems even more likely that primordial binaries play a fundamental role in the BSS formation mechanism. Better information on the abundance of primordial binaries in clusters and their survival rate at a given distance from the cluster center is essential. In 47 Tuc, a recent extensive search for binary stars in the core (Albrow et al. 2001) gave an overall binary frequency of $14\% \pm 4\%$. Figure 21 in Albrow et al. (2001) shows that the binaries appear to be significantly more centrally concentrated with respect to the normal cluster stars, but less concentrated than the BSSs. Hence, if the cluster is in dynamical equilibrium, the CBSSs are among the heaviest visible stellar components in the core of 47 Tuc. Albrow et al. also note that W UMa type stars form a sequence in the CMD like that that would be expected for equal mass binaries. The brightest lie in the BSS region of the CMD. Since W UMa type systems are contact binaries, they may well merge to become BSSs.

Unfortunately, binary populations have been measured in only a few additional clusters (most notably NGC 6752 and NGC 288), and they probably have diverse origins: (1) In the core of NGC 6752 (Rubenstein & Bailyn 1997) the binaries are probably not primordial, since NGC 6752 is such a dynamically evolved cluster (Ferraro et al. 2003a, and references therein); and (2) in the low density cluster NGC 288 (Bellazzini et al. 2002), the binaries are probably primordial. Despite the much longer relaxation time of NGC 288, the binaries have all settled to within the inner half-light radius. The technique used by Rubenstein & Bailyn (1997) and Bellazzini et al. (2002) requires only modest *HST* observation time and should be applicable to any cluster. Even though such studies of the binary populations are painful, we need more.

Clearly, it is desirable to have full BSS surveys for more clusters. It may well be a fluke that the first two clusters to be fully surveyed have bimodal distributions. We have previously pointed out that all properly studied clusters have CBSSs (Ferraro et al. 2003b). The existence of EBSSs in M3 (Sandage 1953) marked the discovery of BSSs. Similarly, there is clear evidence for EBSSs in ground-based CMDs of 47 Tuc (Sills et al. 2000; Grundahl et al. 2002; Kaluzny et al. 1998). Quite possibly, all clusters with significant EBSS populations are bimodal. On the other hand, high-quality CMDs of other clusters like M5 (Sandquist et al. 1996) and M80 (Brocato et al. 1998) show evidence for few if any EBSSs. If more careful studies of such clusters do not reveal a yet undetected EBSS population, we will have to search for a mechanism that produces bimodal radial BSS distributions in some clusters but not in others.

The population of BSSs discovered here opens a new window for the investigation of the origin and the formation mechanism of BSSs in galactic globular clusters. In fact, this discovery suggests that the *peculiar* radial distribution first found in M3 is much more common than was thought. Possibly in a few years we will refer to Figure 5 as the typical radial BSS distribution in stellar aggregates. In the meanwhile let us still refer to it as *peculiar* until its generality can be finally addressed.

We are now exploiting the wealth of information in the large dataset presented here by performing an extensive spectroscopic survey of the BSS population in 47 Tuc using the new multifiber Fiber Large Array Multi-Element Spectrograph (FLAMES) at the ESO Very Large Telescope. These data should be highly informative. For instance, radial velocity determinations for a significant number of EBSSs would help to clarify their origin: if the EBSSs were ejected from the cluster center, their velocity dispersion should be low because they are expected to be observed near the apocenter of an highly elliptical orbit; if EBSSs arise from primordial binaries, the velocity dispersion might be close to the Keplerian velocity (circular orbits that avoid the cluster center might allow the binaries to remain in the exterior) and show small variations due to low-mass companions. The same spectra could lead to many mass estimates; so far the only BSS with a measured mass ($1.7 \pm 0.4\ M_{\odot}$) is in 47 Tuc and was obtained with *HST* (Shara, Saffer, & Livio 1997).

We warmly thank Paolo Montegriffo for assistance during the astrometry procedure and Michela Mapelli and Andrea Possenti for useful discussion. The financial support of the Agenzia Spaziale Italiana (ASI) and the Ministero dell'Istruzione, dell'Università e della Ricerca is kindly acknowledged. This research has made use of the GSCII catalog which has been produced by the Space Telescope Science Institute and the Osservatorio Astronomico di Torino, and also the ESO/ST-ECF Science Archive facility, which is a joint collaboration of the European Southern Observatory and the Space Telescope-European Coordinating Facility. R. T. R. is partially supported by STScI grant GO-8709 and NASA LTSA grant NAG 5-6403.

REFERENCES

Albrow, M. D., Gilliland, R. L., Brown, T. M., Edmonds, P. D., Guhathakurta, P., & Sarajedini, A. 2001, ApJ, 559, 1060
Bailyn, C. D., & Pinsonneault, M. H. 1995, ApJ, 439, 705
Bellazzini, M., Fusi Pecci, F., Messineo, M., Monaco, L., & Rood, R. T. 2002, AJ, 123, 1509
Bolte, M., Hesser, J. E., & Stetson, P. B. 1993, ApJ, 408, L89
Brocato, E., Castellani, V., Scotti, G. A., Saviane, I., Piotto, G., & Ferraro, F. R. 1998, A&A, 335, 929
Buonanno, R., Buscema, G., Corsi, C. E., Ferraro, I., & Iannicola, G. 1983, A&A, 126, 278
Buonanno, R. & Iannicola, G. 1989, PASP, 101, 294
Camilo, F., Lorimer, D. R., Freire, P., Lyne, A. G., & Manchester, R. N. 2000, ApJ, 535, 975
de Marchi, G., Paresce, F., & Ferraro, F. R. 1993, ApJS, 85, 293
Djorgovski, S. 1993, in ASP Conf. Ser. 50, Structure and Dynamics of Globular Clusters, ed. S. G. Djorgovski & G. Meylan (San Francisco: ASP), 373
Djorgovski, S., & Meylan, G. 1993, in ASP Conf. Ser. 50, Structure and Dynamics of Globular Clusters, ed. S. G. Djorgovski & G. Meylan (San Francisco: ASP), 325

Edmonds, P. D., Gilliland, R. L., Heinke, C. O., & Grindlay, J. E. 2003, ApJ, 596, 1177
Ferraro, F. R., D'Amico, N., Possenti, A., Mignani, R. P., & Paltrinieri, B. 2001, ApJ, 561, 337
Ferraro, F. R., Paltrinieri, B., Rood, R. T., & Dorman, B. 1999, ApJ, 522, 983
Ferraro, F. R., Pecci, F. F., Cacciari, C., Corsi, C., Buonanno, R., Fahlman, G. G., & Richer, H. B. 1993, AJ, 106, 2324 (F93)
Ferraro, F. R., Possenti, A., Sabbi, E., Lagani, P., Rood, R. T., D'Amico, N., & Origlia, L. 2003a, ApJ, 595, 179
Ferraro, F. R., Sills, A., Rood, R. T., Paltrinieri, B., & Buonanno, R. 2003b, ApJ, 588, 464
Ferraro, F. R., et al. 1997, A&A, 324, 915 (F97)
Grindlay, J. E., Heinke, C., Edmunds, P. D., & Murray, S. S. 2001, Science, 292, 2290
Grundahl, F., Stetson, P. B., & Andersen, M. I. 2002, A&A, 395, 481
Guhathakurta, P., Yanny, B., Schneider, D. P., & Bahcall, J. N. 1992, AJ, 104, 1790
Holtzmann, J. A., Burrows, C. J., Casertano, S., Hester, J. J., Trauger, J. T., Watson, A. M., & Worthey, G. 1995, PASP, 107, 1065
Howell, J. H., Guhathakurta, P., & Gilliland, R. L. 2000, PASP, 112, 1200
Kaluzny, J., Wysocka, A., Stanek, K. Z., & Krzeminski, W. 1998, Acta Astron., 48, 439
Knigge, C., Zurek, D. R., Shara, M. M., & Long, K. S. 2002, ApJ, 579, 752
Lemon, D. J., Wyse, R. F. G., Liske, J., Driver, S. P., & Horne, K. 2004, MNRAS, 347, 1043
Mapelli, M., Sigurdson, S., Colpi, M., Ferraro, F. R., Possenti, A., Rood, R. T., Sills, A. & Beccari, G. 2004, ApJL, submitted
Momany, Y., et al., 2001, A&A, 379, 436
Montegriffo, P., Ferraro, F. R., Fusi Pecci, F., & Origlia. L. 1995, MNRAS, 276, 739
Pryor, C. & Meylan, G. 1993, in ASP Conf. Ser. 50, Structure and Dynamics of Globular Clusters, ed. S. G. Djorgovski & G. Meylan (San Francisco: ASP), 357
Ratnatunga, K. U., & Bahcall, J. N., 1985, ApJS, 59, 63
Renzini, A., & Buzzoni, A. 1986, in Spectral Evolution of Galaxies, ed. C. Chiosi & A. Renzini (Dordrecht: Reidel), 135
Rubenstein, E. P., & Bailyn, C. D. 1997, ApJ, 474, 701
Sandage, A. R. 1953, AJ, 58, 61
Sandquist, E. L., Bolte, M., Stetson, P. B., & Hesser, J. E. 1996, ApJ, 470, 910
Schechter, P. L., Mateo, M., & Saha, A. 1993, PASP, 105, 1342
Shara, M. M., Saffer, R. A., & Livio, M. 1997, ApJ, 489, L59
Sigurdsson, S., Davies, M. B., & Bolte, M. 1994, ApJ, 431, L115
Sills, A., Bailyn, C. D., Edmonds, P. D., & Gilliland, R. L. 2000, ApJ, 535, 298
Unavane, M., Wyse, R. F. G., & Gilmore, G. 1996, MNRAS, 278, 727
Zaggia, S., Piotto, G., & Capaccioli, M. 1997, A&A, 327, 1004
Zoccali, M., et al. 2001, ApJ, 553, 733